Materials and Design 54 (2014) 553–563

Contents lists available at ScienceDirect

Materials and Design

journal homepage: www.elsevier.com/locate/matdes

Technical Report

Mechanically improved and optically transparent polycarbonate/clay nanocomposites using phosphonium modified organoclay

Supratim Suin, Sandip Maiti, Nilesh K. Shrivastava, B.B. Khatua *

Materials Science Centre, Indian Institute of Technology, Kharagpur 721302, India

ARTICLE INFO

Article history:
Received 6 February 2013
Accepted 22 August 2013
Available online 2 September 2013

ABSTRACT

The present study deals with the properties of polycarbonate (PC)/clay nanocomposites prepared through melt and solution blending at two different clay loadings (0.5 phr and 1 phr) with preserved optical transparency of PC. The organoclay was prepared by exchanging the Na^+ ions presented in the clay galleries of Na-MMT with butyltriphenylphosphonium ($BuTPP^+$) ions, and denoted as BuTPP-MMT. The outstanding thermal stability of the BuTPP-MMT (~1.44 wt% loss at 280 °C, after 20 min), concomitant with the increase in gallery height from 1.24 nm to 1.83 nm, proved its potentiality as nanofiller for melt-blending with PC. The X-ray diffraction analysis (XRD) revealed the destruction of the ordered geometry of aluminosilicate layers in the nanocomposites. However, from direct visualization through transmission electron microscopy, a discernible amount of clay was found to be localised in PC matrix in the 1 phr clay loaded nanocomposites (TEM). The differential scanning calorimetric (DSC) study revealed a nominal increase in glass transition temperature (T_g) of the PC in the nanocomposites. The thermal stability of the nanocomposites was increased with increase in clay loading. The nanocomposites possessed improved tensile strength and modulus than that of the virgin PC and the properties were related to the amount of clay loading and degree of clay dispersion. The dynamic mechanical analysis (DMA) revealed that the storage modulus increased in both the glassy and rubbery region with increase in clay loadings in the nanocomposites. Moreover, the optical transparency of the PC was retained in the PC/clay nanocomposites without development of any colour in the nanocomposites.

1. Introduction

Polymer/clay nanocomposites have attracted many researchers of both industry and academia for its fabulous sets of properties originating from the reinforcement generated from the incorporation of nanoscopic clay layers into the polymer matrix. Such properties in these nanocomposites are associated with the high aspect ratio and surface area of the nanoscopic silicate layers even at very low clay loading [1]. The polymer/clay nanocomposites appear as a material possessing improved tensile properties [2], thermal stability [3], flame retardency [4] and impermeability to gas [5] compared to the unfilled or conventional filler filled composites. The dispersion of the clay layers into the polymer matrix as well as the interaction between polymer and clay are considered to be the determining factor for such improvement in properties. In ideal case, the individual clay platelets are supposed to be fully delaminated into the polymer matrix, resulting largest improvements in properties, because of possibly highest area of interaction between polymer and clay for a particular loading of clay [6]. Intercalated nanocomposites are formed when the interaction between polymer and clay is insufficient to delaminate the clay platelets. The penetration of some of the polymer chains into the clay galleries increases the layer spacing of the clay with moderate increment in property. In conventional composites or microcomposites, the interaction between the polymer and filler is very weak and the filler particles remain in agglomerated form, resulting very nominal improvement in properties. Generally, three methods are used to prepare polymer/clay nanocomposites: (a) *in situ* polymerization of the monomers in the presence of clay [7], (b) melt processing [8–15], and (c) solution casting [16].

In order to incorporate hydrophilic clay silicate layers into the hydrophobic polymer matrix, either the clay or the polymer need to be modified to enhance their compatibility. In practical purpose the first one is chosen, for its simplicity and better dispersion of clay layers into the polymer matrix. To make the clay compatible to the polymer matrix, bulky ions such as quaternary ammonium [8–13], quaternary phosphonium [17–22], and imidazolium [22,23]. are generally incorporated into the clay galleries. The choice of the modifier is based on the processing temperature of the nanocomposites and desired property in the final nanocomposites.

Polycarbonate (PC) is a high performance amorphous engineering thermoplastic possessing outstanding thermal stability, heat distortion temperature (HDT) and optical transparency. The

* Corresponding author. Tel.: +91 3222 283978.
E-mail address: khatuabb@matsc.iitkgp.ernet.in (B.B. Khatua).

0261-3069/$ - see front matter © 2013 Elsevier Ltd. All rights reserved.
http://dx.doi.org/10.1016/j.matdes.2013.08.091

thermal and mechanical properties of polymers are reported to be increased on incorporating inorganic fillers into the polymer matrix. If it can be done without significant loss in optical transparency, PC based composites can be used in a wide application areas. The high processing temperature of PC (280 °C) causes degradation of quaternary ammonium modifier (generally used as modifier) through Hoffmann elimination reaction generating reactive radical [24], which favours degradation of PC matrix through Fries rearrangement [25] converting PC into coloured quinoid form, and thus, results colour in the PC/clay nanocomposites. This sort of degradation of PC matrix is associated with the reduction in molecular weight, mechanical strength, glass transition temperature (T_g), optical transparency and colour development in the final nanocomposites.

Various attempts have been reported to prepare PC/clay nanocomposites via incorporation of different modified clays through both the melt and solution blending process. Brittain et al. [8] applied ring opening polymerization technique to prepare PC/clay nanocomposites with intercalated-exfoliated morphology, using low molecular weight cyclic carbonate oligomers and ditallow dimethyl quaternary ammonium substituted montmorillonite. Han [9] reported that the higher degree of clay exfoliation and good compatibility between PC and clay in the twin-screw extruded PC/clay nanocomposites was caused by the H-bonding between the active functional group of modifier and the carbonyl group presented in PC. Paul et al. [10] investigated the effect of molecular weight of PC and the structure of the organoclay on the morphology and properties of PC/clay nanocomposites. The higher degree of dispersion of the clay platelets into the high molecular weight PC was achieved by the high shear force generated during the melt processing of high molecular weight PC. Their study also revealed that the reduction of molecular weight and appearance of colour in the melt blended PC/clay nanocomposites depends on residence time in the extruder, chemical structure of the modifier, and the iron content of the clay [11]. Okamoto et al. [12] investigated the effect of a compatibilizer during melt intercalation of the PC/clay nanocomposites. They reported that the mechanical property of the PC was increased on incorporating clay into the PC/clay nanocomposites. Their study also revealed that, the morphology of the clay in the nanocomposites and degradation of the PC during processing can be varied by changing the surfactants in the modified clay and the compatibilizer. Hsieh et al. [13] studied the effect of clay loading on the mechanical performance and rheological properties of melt-intercalated PC/clay nanocomposites. They concluded that, with increase in the clay loading the T_g and molecular weight of the PC in the nanocomposites were decreased during melt compounding due to the degradation of the of PC matrix. Nevalainen [14] studied the morphology and mechanical properties of twin screw extruded PC/clay nanocomposites, using two different ammonium modified clays. The tensile strength and young modulus of the nanocomposites were increased, whereas, impact strength was decreased on incorporating the clay into the virgin PC, irrespective of the nature of modifier. On incorporating clay into the PC, a transition from ductile to brittle was also evident from their study. Zhang et al. [15] studied the efficiency of epoxy resin in compatibilization of the melt-intercalated PC/clay nanocomposites. Addition of small amount of epoxy resin favoured the dispersion of clay platelets into the PC matrix, whereas, the epoxy at higher loading acted as plasticizer causing undesirable degradation of the PC matrix. Swaminathan [22] have recently reported the preparation of exfoliated PC/clay nanocomposites using phosphonium and imidazolium modified organoclay via *in situ* melt polycondensation. In spite of the occurrence of thermally stable bisphenol functionality in the modifier, the final PC/clay nanocomposites appeared dark brown in colour.

The literature on PC/clay nanocomposites deals mainly with the morphological and mechanical properties of the nanocomposites in the presence of various modified clays. However, a very small stress has been given towards the optical transparency and colour issues of the PC/clay nanocomposites. Here, we report the preparation of optically transparent PC/clay nanocomposites through conventional melt and solution blending process and properties of the nanocomposites. The effect of blending technique on the morphology, mechanical and optical properties and colour issues are described in detail in the manuscript.

2. Experimental details

2.1. Materials used

Commercial grade bisphenol-A polycarbonate (PC) (Lexan 143, MFI ≈ 10.5 g/10 min at 300 °C and 1.2 kg load) used in this study was supplied by SABIC Innovative Plastics. The unmodified nanoclay (sodium montmorillonite, Na-MMT) was purchased from Southern Clay Products, Inc., USA. The cation exchange capacity (CEC) value of the supplied Na-MMT is 92 mequiv/100 gm of clay. The organic modifier, butyl triphenylphosphonium bromide (BuTPP-Br) was procured from Sigma–Aldrich. Methanol and dichloromethane were obtained from Merck Germany.

2.2. Modification of the clay

The modification of the unmodified clay, Na-MMT was done through the ion exchange reaction using BuTPP-Br in water medium. In a 500 ml beaker, 2.5 g Na-MMT was dispersed in 250 ml de-ionized water and ultrasonicated at room temperature for 1 h to break the layered structure of clay in the water medium. The resulting Na-MMT/water suspension was then transferred in a 2L three neck round bottom flask (R. B. flask) containing 500 ml water and stirred for 45 min, using an overhead stirrer. The temperature of the reactor was maintained at 80 °C throughout the ion exchange reaction. Based on the CEC value of the Na-MMT (given by the supplier), slightly higher amount (~1 g) of the quaternary phosphonium salt (BuTPP-Br) was dissolved in 50 ml de-ionized water. The higher amount of BuTPP-Br facilitated the modification of the Na-MMT clay as much as possible. The BuTPP-Br solution was then added drop wise over a period of 10 min to the dispersed Na-MMT suspension in round bottom flask under stirring condition. The reaction was allowed to continue for another 2 h to complete the ion exchange reaction. The settling down of the clay agglomerates in the reaction flask indicated the completion of the reaction. The incorporation of the organic moiety inside the clay galleries was responsible for the generation hydrophobicity in the clay, which resulted in settling down of the clay. The resulting agglomerates were then filtered by using vacuum pump and washed in a vessel containing 250 ml of water under stirring at 80 °C for 20 min to remove the undesired impurity (NaBr and unexchanged butyltriphenylphosphonium bromide). The organoclay-water suspension was re-filtered. The washing process was continued until the filtrate was free from bromide ion, as examined by a dilute $AgNO_3$ solution. The final washing was done by 250 ml methanol to eliminate the excess butyltriphenylphosphonium ion presented in the clay galleries. The moist clay was first air-dried and then under vacuum at 80 °C for 12 h. The oven-dried clay aggregates were then grinded to fine powder with the help of mortar and pastel. The schematic for the modification of the clay is shown in Fig. 1.

2.3. Preparation of the PC/clay nanocomposites

Two different blending techniques (melt and solution blending) were used for the preparation of PC/clay nanocomposites at two

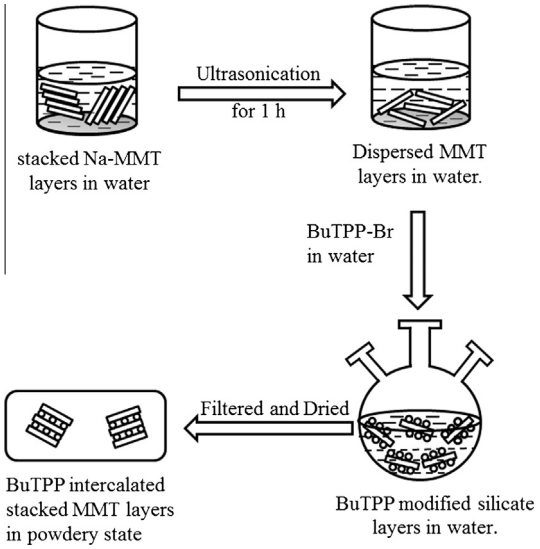

Fig. 1. Organic modification of Na-MMT.

different loadings (0.5 and 1 phr) of BuTPP-MMT, as described below.

2.3.1. Melt mixing

To avoid any moisture induced thermal degradation of the components, calculated amount of PC and the clay were dried in a vacuum oven at 100 °C for 12 h before melt mixing. Melt-mixing of the PC and BuTPP-MMT clay was done in an internal mixer (Brabender Plasticorder with chamber capacity of 20 cc; S.C. Dey & Co., Kolkata, India) at 280 °C, 60 rpm for 15 min. Finally, the melt-mixed PC/BuTPP-MMT nanocomposites were injection molded (applied pressure 4 kg/cm^2) into desired shapes at 280 °C for further characterizations.

2.3.2. Solution casting

In a 250 ml beaker, 20 g PC was dissolved in 100 ml of dichloromethane (DCM) at room temperature. In another 250 ml beaker, calculated amount (0.1 and 0.2 g) of the modified clay was well dispersed in 60 ml DCM by ultrasonic probe sonicator at room temperature. After 30 min of sonication, the PC/DCM solution was gradually added into the clay/DCM suspension for a period of 5 min under constant sonication. The sonication of PC/BuTPP-MMT solution mixture was continued for another 30 min. Finally, the mixture was stirred for 15 min at 60 rpm with a magnetic stirrer at room temperature and the mixture was transferred in a Petri-dish. The composite flakes were obtained after the evaporation of the DCM in air. The final solution blended nanocomposites material was obtained after complete removal of the solvent in vacuum oven.

3. Characterizations

3.1. Fourier Transform Infrared (FTIR) spectroscopy

The FTIR spectral analysis of the Na-MMT (unmodified clay) and phosphonium modified clays were done on a NEXUS 870 FTIR (Thermo Nicolet) instrument. The pellets were made by grinding the clays with spectroscopic grade KBr and introducing into the pelletizer. FTIR spectra of both the clays were recorded using the pellets in the range of 4000–400 cm^{-1}.

3.2. X-ray diffraction analysis

The d-spacing (gallery height) of the unmodified Na-MMT and the modified BuTPP-MMT clays and their nanocomposites with PC was measured by using a X-ray diffractometer, (Panalytical High Resolution XRD-I, PW 3040/60) with nickel-filtered Cu Kα line (λ = 0.15404 nm) operated at an accelerating voltage of 40 kV and 30 mA, at a scanning rate of 0.5°/min. The distance between sample and detector was 400 mm. The gallery height of the ordered layered assembly of the clay was calculated by using the Bragg's law ($n\lambda = 2d\sin\theta$), where d represents the distance between the d_{001} planes in the ordered structure, λ is the wave length of the incident wave and θ is the angle between the incident wave and the scattering planes, and n is an integer.

3.3. TEM analysis

The morphological studies of the nanocomposites were also done by direct visualization of the clay silicate layers in the PC by transmission electron microscopy (HRTEM: JEM-2100, JEOL, Japan) operating at an accelerating voltage of 100 kV. The PC/clay nanocomposites samples were ultramicrotomed under cryogenic condition (cryo-cut) with a thickness of 60–100 nm. Since the clay possesses much higher electron density than the polymer (PC), no staining was required and the clay platelets appeared dark in the TEM images. Energy dispersive X-ray spectroscopy (EDS) analysis of the Na-MMT and the BuTPP-MMT were carried out by casting the dispersed samples on respective Cu grids.

3.4. Gas permeation properties

The gas permeation responses of the neat PC and PC/BuTPP-MMT nanocomposites films (thickness 60–80 μm) were studied using the automated Diffusion Permeameter (DP-100-A, Porous Materials, Inc., USA) at 35 °C and 3.5 bar of applied gas (nitrogen, N_2 gas) pressure. A constant pressure of 3.5 bar was maintained throughout the experiment and the effective permeation area was 5.069 cm^2. The incorporated gas was applied instantaneously to the upstream side of the film and in the downstream side a reservoir of constant volume (119 cm^3) was connected with a pressure transducer to monitor the total amount of gas which passed through the polymer film. The permeability coefficients were calculated from the following equation:

$$p = \left[\frac{VdT_0}{Ap_ip_0T}\right]\left(\frac{dp}{dt}\right) \quad (1)$$

where T_0 and p_0 stands for the standard temperature (T_0 = 273.15 K) and pressure (p_0 = 1.013 bar), T is the temperature during measurement, d is the thickness of the film and $(dp/dt)_s$ was obtained from the slope of the increments of downstream pressure vs. time plot.

The effective diffusion coefficient D was calculated from the time-lag, according to the following Eq. (2). The time-lag values were varied between 5 and 10 min depending on the structure of polymer and penetrating gas under experiment.

$$D = \frac{d^2}{6\theta} \quad (2)$$

3.5. Differential scanning calorimetry (DSC)

The T_g of the neat PC and its nanocomposites with BuTPP-MMT was determined with differential scanning calorimetry (DSC-200 PC, NETZSCH), using 10–12 mg of sample in nitrogen atmosphere. The samples were first heated from room temperature to 330 °C and held at 330 °C for 5 min to remove the moisture and previous

thermal history. Then cooling was done to room temperature and reheated to 330 °C. The T_g of the samples was determined from the second heating scans. The heating and cooling rate was 10 °C/min throughout the test process.

3.6. Thermogravimetric analysis (TGA)

The stability of the neat PC and PC/BuTPP-MMT nanocomposites against thermal decomposition was investigated using a TGA V 50 IA Dupont 2100 thermo gravimetric analyzer in nitrogen in the temperature range of 30–800 °C, with a heating rate of 10 °C/min. The isothermal TGA run for the organoclay (BuTPP-MMT) was carried out at 280 °C to examine the thermal stability of the modified clay at the processing temperature of the PC.

3.7. Tensile properties

The tensile test for pure PC and its nanocomposites with BuTPP-MMT was performed following ASTM: D-638 on dumb-bell shaped injection molded samples using a Tinius Olsen H 50 KS (universal testing machine) at room temperature with a gauge length of 23 mm, width 4.8 mm, thickness 2 mm and crosshead speed of 5 mm/min. The reported tensile values are the average of the results for tests run on at least five specimens.

3.8. Dynamic mechanical analysis (DMA)

The thermo-mechanical properties (storage modulus) of the pure PC and the PC/BuTPP-MMT nanocomposites was measured by a dynamic mechanical analyzer (DMA 2980 model, TA Instruments Inc., USA), using injection molded impact bar samples. The dynamic temperature spectra of the PC, as well as the PC/BuTPP-MMT nanocomposites were obtained in tension film mode at a constant vibration frequency of 1 Hz, temperature range of 40–170 °C at a heating rate of 5 °C/min in nitrogen atmosphere. The dimension of the specimen was $32 \times 12.5 \times 3.5\ mm^3$.

3.9. UV–vis spectroscopy

The UV–vis spectroscopic analysis was carried out to examine the optical transparency of the pure PC and melt and solution blended PC/BuTPP-MMT nanocomposites using solid films. The melt compounded films were prepared by compression molding at a constant pressure. To prepare the solution casted films, 0.5 g of pure PC and the solution casted nanocomposites were dissolved separately in 15 ml dichloromethane (DCM). These composite containing DCM solutions were poured separately over different Petridishes having uniform surface. The slow evaporation of DCM at room temperature yielded the solid films. To compare the optical transparency of the nanocomposites films with PC films, the percent transmittance was measured as a function of wavelength by using Perkin Elmer, Lambda 750 spectrophotometer.

4. Results and discussion

4.1. Analysis of the BuTPP-MMT clay

4.1.1. FTIR study

Fig. 2 represents the FTIR spectra of the pure Na-MMT and the modified clay. As observed, the pure Na-MMT (Fig. 2a) gave rise the characteristic bands at 3620, 1040, 516 and 460 cm^{-1} corresponding to the different mode of bond vibrations of the aluminosilicate compound. The highly intense band at 3620 cm^{-1} corresponds to the 'O–H' stretching vibration. The bands at 1040 and 460 cm^{-1} are related to the 'Si–O' stretching and 'Si–O–Si' bending vibrations, respectively. The peak at 516 cm^{-1} corresponds to the 'Al–O' stretching vibration. The presence of the proper moiety in the modified can be verified through the vibrational bands related to the particular group in the FTIR spectrograph along with the characteristic bands related to aluminosilicate cluster in MMT-clay. The peaks at 1430 and 1115 cm^{-1} are related to the in plane and out of plane bending of the PPh_3, respectively. Appearance of two relatively weak peaks at 2860 and 2920 cm^{-1} could be related to C–H symmetric and asymmetric stretching of methylene ($–CH_2–$) group presented in the modifier. Thus, the IR spectroscopic analysis of the unmodified clay (Na-MMT) and the modified clay (BuTPP-MMT) revealed the inclusion of butyl triphenyl phosphonium moiety (phosphonium modifier) in the clay galleries of Na-MMT during the ion exchange reaction.

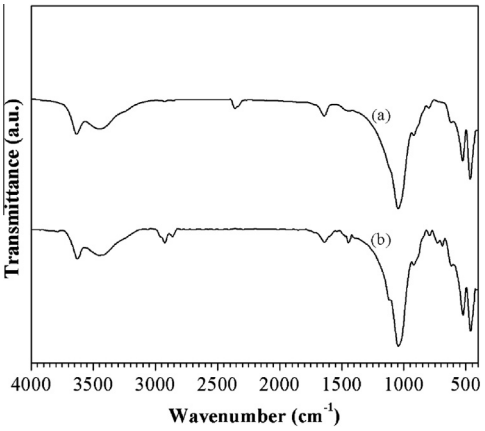

Fig. 2. FTIR spectra of (a) Na-MMT, (b) BuTPP-MMT.

4.1.2. EDS analysis of the BuTPP-MMT clay

The presence of organic moiety in the modified BuTPP-MMT clay was verified through the elemental analysis (EDS) of the pure Na-MMT and the modified BuTPP-MMT. The EDS spectra of the clay before (Fig. 3a) and after (Fig. 3b) the ion exchange reaction is depicted in Fig. 3. From the EDS spectrographs it can be seen that, the major components of Na-MMT are oxygen, aluminium and silicon with traces amount of sodium, calcium, magnesium and iron. The disappearance of sodium and appearance of carbon, phosphorus (along with the oxygen, aluminium, silicon, magnesium and iron) in the EDS spectra of the modified clay clearly indicates the replacement of sodium ions in the clay galleries of the unmodified clay with the quaternary phosphonium ion after ion exchange reaction.

4.1.3. XRD analysis of the BuTPP-MMT clay

The XRD patterns of the unmodified Na-MMT clay and the phosphonium modified BuTPP-MMT clay are represented in Fig. 4. The Na-MMT shows the characteristic peak (Fig. 4a) of the clay at $2\theta \approx 7.12$, corresponding to the gallery height (d_{001} spacing) of ≈1.24 nm. The d_{001} peak for the BuTPP-MMT clay (Fig. 4b) was shifted to a lower region ($2\theta \approx 4.8$), indicating the increase in d_{001}-spacing (≈1.83 nm) in the modified clay. An increase in d_{001}-spacing from 1.17 nm to 1.85 nm was previously found by Han et al. [9], when the organic moiety replaced the intra-gallery Na^+ of cloisite-Na^+, resulting cloisite 30B. Our result unambiguously led us to assume the replacement of smaller Na^+ ions by bulky quaternary phosphonium ions inside the clay galleries that resulted in the increase in the gallery height of the MMT layers during ion-exchange reaction.

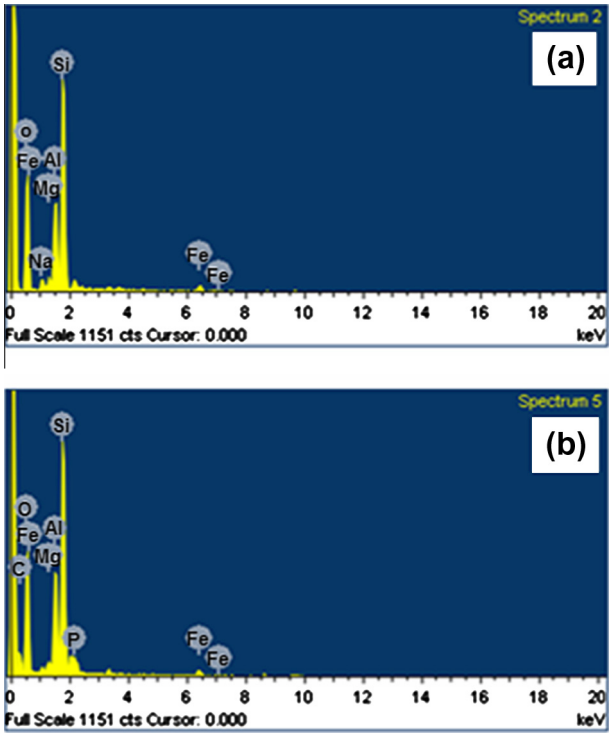

Fig. 3. EDS spectra of (a) Na-MMT, (b) BuTPP-MMT.

4.1.4. Thermal stability of the modified clay

To investigate the stability of the BuTPP-MMT at the processing temperature of PC (280 °C), the isothermal TGA scan of the modified clay was carried out at the said temperature in air atmosphere. The BuTPP-MMT was allowed to stand for 20 min in isothermal condition and the mass remaining during this period was plotted against time (Fig. 5). After 20 min, the plot showed a residual mass of ≈98.56 wt%, indicating only 1.44 wt% of the clay was degraded during this period. This study indicates the suitability of BuTPP-MMT as potential nanofiller in the preparation of PC/clay nanocomposites without any thermal degradation of the clay.

4.2. Analysis of the PC/BuTPP-MMT clay nanocomposites

4.2.1. XRD analysis

Fig. 6 shows the XRD patterns of the BuTPP modified clay and its nanocomposites prepared through both the solution and melt

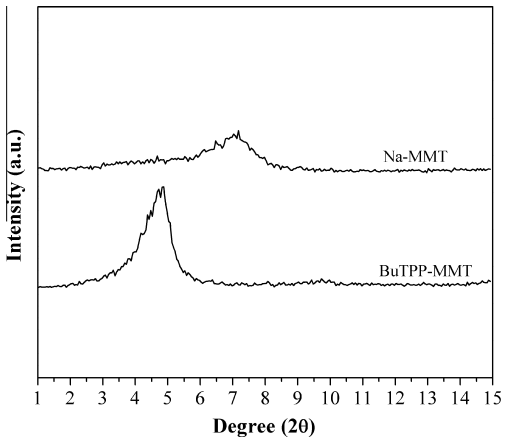

Fig. 4. XRD patterns of the unmodified and modified clay.

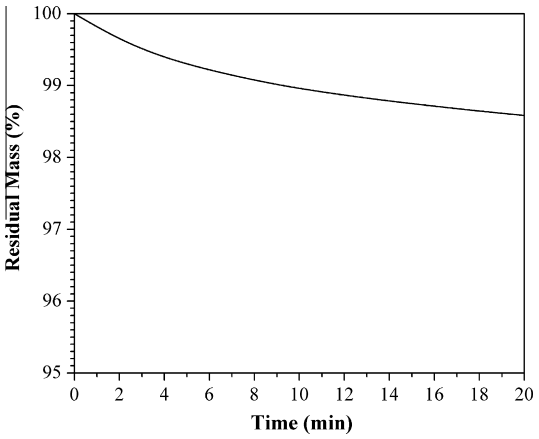

Fig. 5. Isothermal TGA scan for BuTPP-MMT.

blending processes at two different loadings (0.5 phr and 1 phr). Irrespective of the blending techniques, the characteristic peak (Fig. 6a) of the BuTPP-MMT (at $2\theta \approx 4.8°$) was disappeared in the nanocomposites. These XRD results are indicative to the fact that the ordered structure of the clay was destroyed, resulting a well exfoliated morphology in the PC/BuTPP-MMT nanocomposites. The reason behind exfoliation in the melt blending process can be interpreted as the high shear force generated from the mixing of high molecular weight PC during melt blending process. In solution blending process, the clay tactoids are first dispersed in the DCM under ultrasonication followed by the mixing with the dissolved PC in the same solvent. The lower loading of the BuTPP-MMT clay does not allow the individual platelets to aggregate, and hence resulted in a well exfoliated morphology. However, the morphological studies are always incomplete without direct visualization through electron microscopy.

4.2.2. TEM analysis

The dispersion and distribution of the clay silicate layers in the PC matrix of the nanocomposites was studied through direct visualization under TEM. The microstructure of the clay layers in the PC matrix, as observed in TEM, is given in Fig. 7. As can be seen, irrespective of the method of composites preparation, the BuTPP-MMT clay platelets were homogeneously distributed throughout the matrix phase of the nanocomposites at 0.5 phr clay loading. The ordered geometry of the clay platelets were destroyed with the

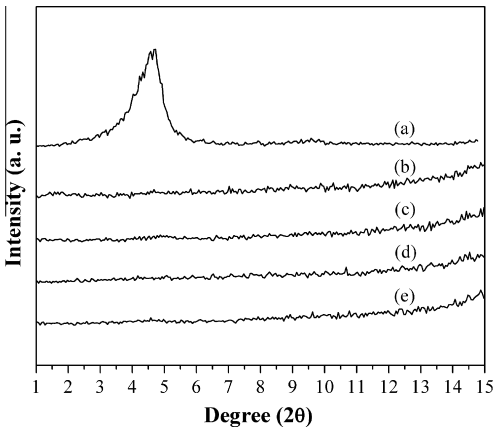

Fig. 6. XRD plots of (a) BuTPP-MMT; melt-blended PC/BuTPP-MMT nanocomposites with: (b) 0.5 phr clay, (c) 1 phr clay; solution-blended PC/BuTPP-MMT nanocomposites with: (d) 0.5 phr clay, and (e) 1 phr clay.

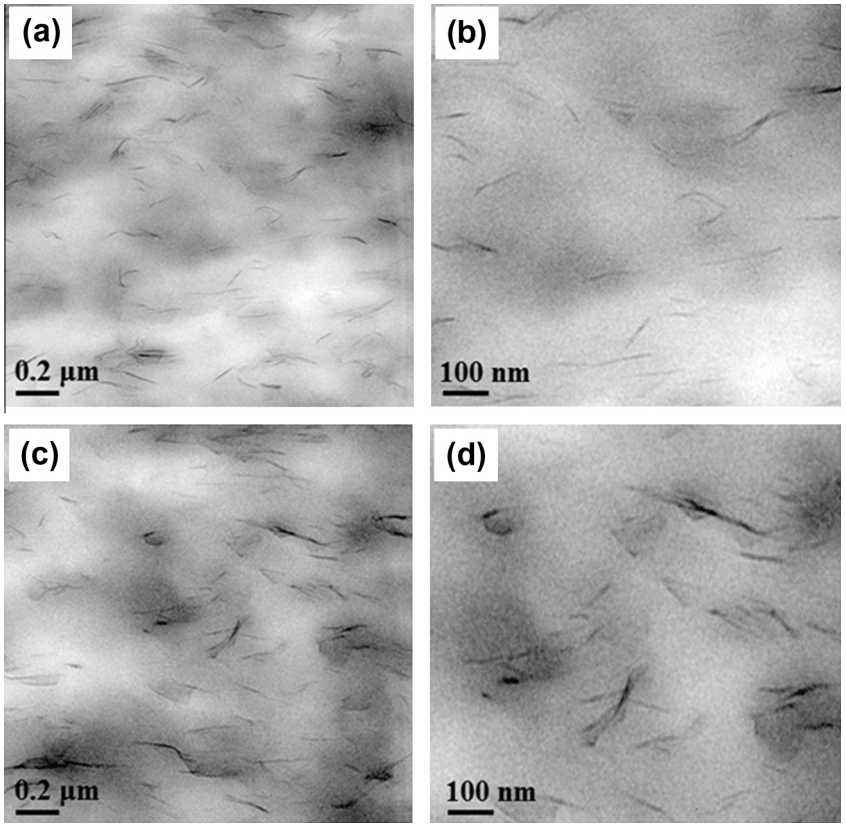

Fig. 7. HRTEM images of 0.5 phr (a and b) and 1 phr (c and d) clay loaded PC/BuTPP-MMT nanocomposites at two different magnifications: (a and c) low magnification, (b and d) high magnification. In all the cases the nanocomposites were melt blended.

formation of highly delaminated and randomly distributed individual clay platelets, indicating the disordered exfoliation of the clay platelets in the 0.5 phr clay loaded melt and solution blended nanocomposites (Fig. 7a). The good dispersion and distribution of clay silicate layers in the PC matrix at 0.5 phr clay loading can be clearly seen at higher magnification (Fig. 7b). Such high degree of exfoliation was previously found by Han et al. [9] and Swaminathan [22] in case of PC/clay nanocomposites. We assume that, the increase in gallery height in the BuTPP-MMT (as observed in XRD analysis of the clay) promoted the intercalation of the PC chains inside the clay galleries, followed by successive delamination of the silicate layers under high shear force (kinetically favourable) during melt-mixing. Moreover, with increase in clay loading (from 0.5 phr to 1 phr), discernible amount of platelets were appeared as aggregated while most of the clay platelets were randomly distributed (Fig. 7c). However, the higher magnification image (Fig. 7d) of the 1 phr clay loaded nanocomposites showed that the clay platelets were not aggregated, rather than close enough and appeared to be aggregated.

4.2.3. Gas permeation properties: theoretical models based on orientation of clay platelets

Beforehand, the XRD and TEM analysis revealed the presence of high degree of dispersion and distribution of clay platelets in the PC matrix of PC/BuTPP-MMT nanocomposites. However, the actual state of dispersion of clay platelets in the matrix phase can be concluded from different theoretical models based on the gas permeation behaviour.

The gas permeation behaviour in polymer/clay nanocomposites is generally governed by three main factors: the volume fraction of the clay platelets; the orientation of the platelets relative to the diffusion direction and their aspect ratio. The gas permeation properties in a homogeneous virgin polymer matrix are generally governed by the solubility/diffusion mechanism. The solubility coefficient (S) describes the interaction between polymer and penetrant, the thermodynamic aspect of the transport, whereas, the diffusion coefficient (D) describes the kinetic aspect of the transport. It is generally accepted that the gas transport mechanism within the polymer matrix is followed by the Fick's law. According to fickian transport mechanism, the permeability coefficient (P) can be expressed by the following law:

$$P = DS \tag{3}$$

This equation is also valid for the gas transport properties of the nanocomposites, consisting of permeable polymer phase in which impermeable nanofiller particles are dispersed. The solubility coefficient in the nanocomposites is defined as:

$$S = S_0(1 - \phi) \tag{4}$$

where S and S_0 stand for the solubility coefficients in the nanocomposites and pure polymer, respectively, and ϕ is the filler volume fraction.

As the gas molecules experience hindrance from the impermeable platelets presented in the matrix polymer, it has to follow a more tortuous path, resulting in a decrease in the diffusion rate through the nanocomposites membrane:

$$D = \frac{D_0}{\tau} \tag{5}$$

where D_0 and D are diffusion coefficients of the virgin polymer and the nanocomposites, respectively, and τ is the tortuosity factor. Combining Eqs. (3)–(5), the expression for the relative permeability can be written as:

$$\frac{P}{P_0} = \frac{1 - \phi}{\tau} \tag{6}$$

Table 1
Various theoretical models concerning the dispersion of impermeable flakes in permeable polymer.

Model	Assumed geometry	Dispersion type	Relative permeability (p/p_0)
Nielsen [26]	Ribbon	Regular array	$\frac{(1-\phi)}{(1+\alpha\phi/2)}$
Cussler [27]	Ribbon	Regular array	$\frac{(1-\phi)}{1+(\alpha\phi)^2/4}$
	Ribbon	Random array	$\frac{(1-\phi)}{(1+\alpha\phi/3)^2}$
Yang and Cussler [28]	Hexagonal flake	Random misalignment of successive layers	$[1+\frac{2}{27}(\frac{\alpha^2\phi^2}{1-\phi})]^{-1}$
Gusev and Lusty [29]	Disk	Random dispersion of non-overlapping disks	$\frac{(1-\phi)}{\exp[(\alpha\phi/3.47)^{0.71}]}$
Fredrickson and Bicerano [30]	Disk	Random array	$\frac{(1-\phi)}{4[(1+x+0.1245x^2)/(2+x)]^2}$ where $x=\pi\alpha\phi/2\ln(\alpha/2)$

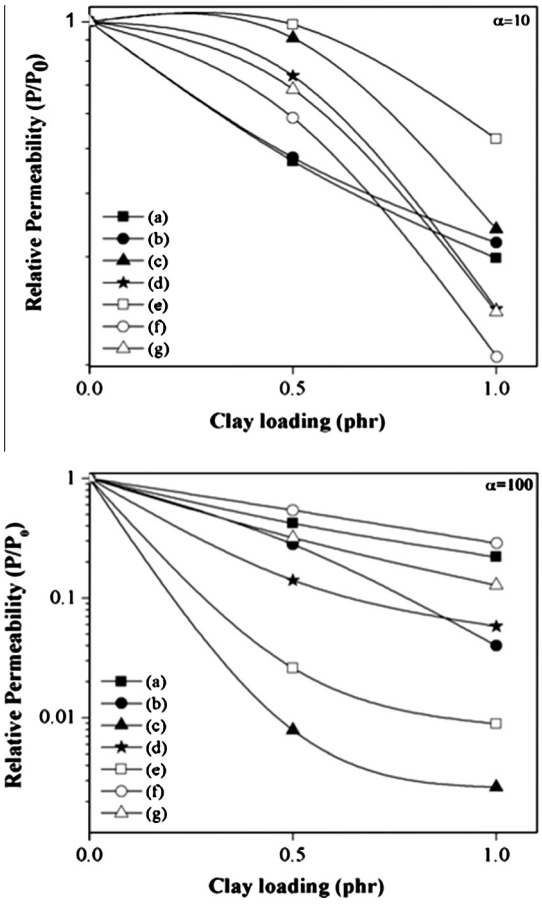

Fig. 8. Variation of relative permeability with clay loading for the experimental and considering different models by: (a) experimental, (b) Nielsen, (c) Cussler (regular array), (d) Cussler (random array), (e) Yang and Cussler, (f) Gusev and Lusty, and (g) Fredrickson and Bicerano.

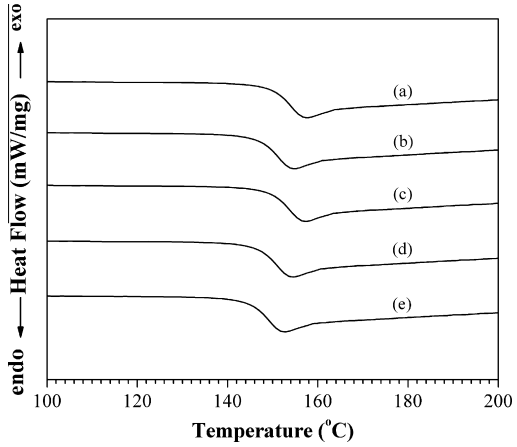

Fig. 9. DSC thermograms of (a) pure PC, melt-blended PC/BuTPP-MMT nanocomposites with: (b) 0.5 phr clay, (c) 1 phr clay; solution-blended PC/BuTPP-MMT nanocomposites with: (d) 0.5 phr clay, and (e) 1 phr clay.

Several models have already been proposed [26–30] in the literature describing the effect of tortuosity as well as the decrease in permeability, resulting from the dispersion of impermeable fillers in the polymer matrix. Here, we deals with the models concerned with only monodispersed impermeable objects. The various proposed models along with the dispersed phase geometry, dispersed state and expression for relative permeability are summarised in Table 1.

The literature based on the gas permeation behaviour of the polymer/clay nanocomposites revealed that, the gas barrier properties is dependent on the tortuosity effect resulting from the dispersion of the impermeable clay layers in the matrix phase, not on the nature of gas. Thus, our study was limited for a particular gas (nitrogen, N_2 gas). Moreover, the aspect ratio (α), a major parameter in the different modelling approach, was reported in the literature to be varied in between 10 and 100 for the montmorillonite clay [31]. To avoid complexity in measuring α, here we consider only the extreme values of α.

The variation of relative permeability with clay loading is depicted in Fig. 8. As observed, the Nielson model lies very much to that of experimental plot at lower limit of α, whereas, at the upper limit the experimental plot was followed by the Gusev and Lusty model and Fredrickson and Bicerano model. Nielson model tells about the regular array of ribbon like clay. On the contrary, random dispersion of non-overlapping disks was assumed by Gusev and Lusty model and Fredrickson and Bicerano model. As inference, regular array of clay at lower α and random dispersion of clay at higher α can be concluded from the modelling approach.

4.2.4. DSC study

T_g is considered to be a very important parameter of polymer composites, which indirectly gives some idea on the morphology as well as the extent of degradation of polymer matrix (if any) caused by the dispersed filler particles. Fig. 9 represents the DSC endotherms of virgin PC and PC/BuTPP-MMT nanocomposites at different clay loadings (0.5 phr and 1 phr), prepared through two different blending techniques. The T_g of the virgin PC was appeared at ≈148 °C, consistent with the T_g reported for Lexan 143 PC. The confinement of the polymer chains into the clay galleries generally leads to an increase in the T_g, in case of intercalated polymer/clay nanocomposites [32,33]. However, a negligible change in T_g of the PC was observed in the case of 0.5 phr clay loaded PC/BuTPP-MMT nanocomposites in both the melt and solution blended nanocomposites (≈150 °C). The delamination of the clay platelets in the

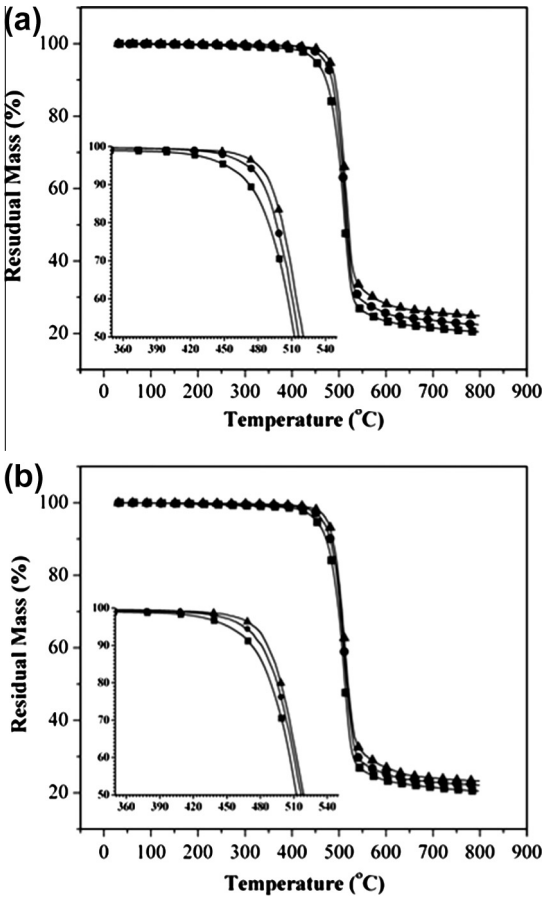

Fig. 10. TGA thermograms of (■) pure PC and its (a) melt blended, (b) solution blended nanocomposites with (●) 0.5 phr BuTPP-MMT and (▲) 1 phr BuTPP-MMT.

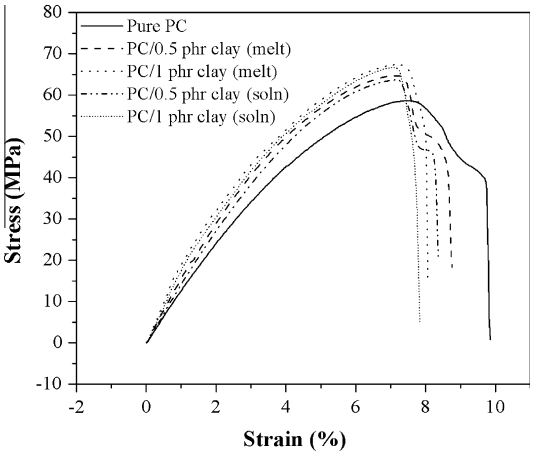

Fig. 11. Stress–strain plots of neat PC and PC/BuTPP-MMT nanocomposites.

PC matrix failed to restrict the bond segmental motion of the PC chains, which could be an effective reason for the nominal increase in T_g. Thus, substantial distribution and dispersion of clay platelets into the PC matrix was indirectly supported by the T_g value, consistent with the XRD and TEM analysis. Moreover, with increase in clay loadings (from 0.5 to 1 phr) the T_g of the PC/BuTPP-MMT nanocomposites was shifted to ≈152 °C for both the melt and solution blended nanocomposites.

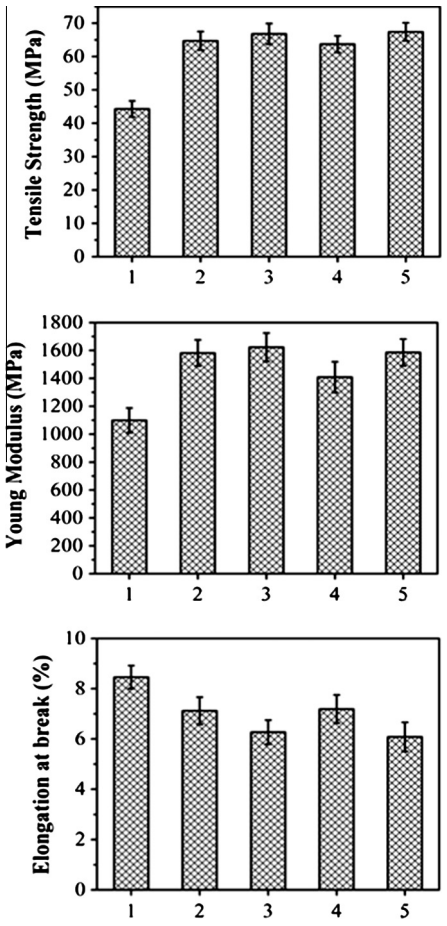

Fig. 12. Mechanical property (tensile strength, Young modulus and elongation at break) plots of (1) pure PC, (2) PC/0.5 phr BuTPP-MMT (melt blended), (3) PC/1 phr BuTPP-MMT(melt blended), (4) PC/0.5 phr BuTPP-MMT (solution blended), and (5) PC/1 phr BuTPP-MMT (solution blended).

4.2.5. TGA analysis

The thermal stability of the polymer/clay nanocomposites is usually governed by the inorganic content of the nanocomposites, as well as, the stability of the organic surfactant ions present in the clay galleries. The dynamic TGA scans of the neat PC and its nanocomposites with different proportion of BuTPP-MMT, prepared through both the blending techniques are plotted in Fig. 10. From the TGA plots the onset degradation temperature (T_0, corresponding to 5 wt% loss) and T_{50} (temperature corresponding to 50 wt% loss) were measured. As can be seen, irrespective of the blending procedure, the T_0 and T_{50} were increased with increase in the clay loading in the PC/BuTPP-MMT nanocomposites. For instance, on incorporating 0.5 phr clay, the T_0 of neat PC (≈449 °C) was reached to ≈469 °C and ≈466 °C for melt blended and solution blended PC/BuTPP-MMT nanocomposites, respectively. However, doubling the clay loadings increased the T_0 by ≈30 °C to that of neat PC in the melt and solution blended nanocomposites. Similar trend was followed in case of T_{50} in the PC/BuTPP-MMT nanocomposites prepared through both the blending techniques. The T_{50} of the virgin PC (≈511 °C) was appeared at ≈516 °C and ≈522 °C for the 0.5 phr and 1 phr clay loaded PC/BuTPP-MMT nanocomposites, respectively. Hsieh et al. [13] found a decrease in thermal stability with increase in clay loadings in PC/clay nanocomposites. This can be attributed to the degradation of PC matrix during melt blending. In our case, the thermal stability of the PC/BuTPP-MMT nanocomposites was increased with increase in clay loading. This sort of increase in thermal stability in the PC/BuTPP-MMT nanocomposites

can be explained in terms of the shielding effect of the clay platelets along with the inherent flame retardant property of the phosphonium modified organoclay [34]. Moreover, the clay presented in the nanocomposites restricted the intimate contact of the heat with the polymer, and thus reduced the diffusion of heat into the bulk of the nanocomposites [35]. The increase proportion of BuTPP-MMT in the PC/BuTPP-MMT nanocomposites thus creates greater shielding effect (originating from the greater inorganic content), leading to the increase in thermal stability. Interestingly, thermal degradation behaviour of both the melt and solution blended nanocomposites followed similar trend, suggesting the presence of almost similar clay morphology in these nanocomposites, indirectly supporting the previously discussed XRD and TEM results.

4.2.6. Mechanical properties

Fig. 11 represents the stress–strain behaviour of pure PC and PC/BuTPP-MMT nanocomposites at different clay loadings, prepared through both the solution and melt blending techniques. As can be seen, the plot of pure PC resembles to hard and tough material with moderate elongation. The incorporation of clay into the polymer matrix increases the tensile stress along with significant decrease in elongation. This study also revealed that the mechanical properties of the nanocomposites was not dependent very much on the blending techniques, rather than customized by the amount of incorporated organoclay.

The mechanical properties (tensile strength, young modulus and elongation at break) of the pure PC and its nanocomposites at different clay loadings are depicted in Fig. 12. As observed, the tensile strength and Young modulus of pure PC was increased by ≈50% and ≈40%, respectively, on incorporating 0.5 phr clay into the PC matrix. The increase in clay loading did not affect very much on the mechanical properties, suggesting relatively poor dispersion of organoclay at higher loading. The larger interacting area between PC and clay platelets in the well exfoliated clay morphology might be the possible cause for such high improvement in mechanical properties at such a lower clay loading [36]. Moreover, the elongation at break was gradually decreased with increase in clay loadings in the PC/BuTPP-MMT nanocomposites. The increase in stress concentration with increase in clay loading into the PC matrix might be responsible for the increase in brittleness in the nanocomposites [37].

Fig. 13 represents the variation in storage modulus with temperature of the pure PC and its nanocomposites at different clay loadings. As evident, the storage modulus of both the melt and solution blended PC/BuTPP-MMT nanocomposites was superior to that of the pure PC in both the rubbery and glassy regions. The increase in storage modulus with increase in clay loading was also found previously in the literature [38,39]. The increment in storage modulus at such a lower clay loading can be explained in terms of higher reinforcing effect, originating from the high aspect ratio delaminated clay platelets which, in turn, help to transfer the stress at the interface [40]. As the clay platelets were not dispersed well in higher clay loadings the increment in storage modulus is not so pronounced, as in case of 0.5 phr clay loading.

The variation of damping factor ($\tan\delta$) with temperature for both the melt and solution blended nanocomposites is depicted in Fig. 14. The T_g values of polymer in the nanocomposites can also be calculated from the peak value of $\tan\delta$. As evident from the curve, the T_g of pure PC (≈152 °C) was increased to ≈154 °C for

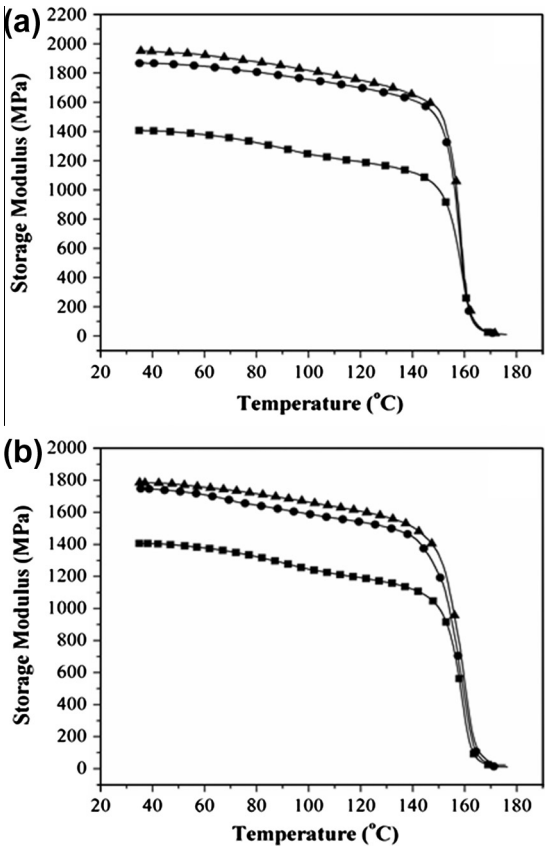

Fig. 13. Storage modulus plots of (■) pure PC and its (a) melt blended, (b) solution blended nanocomposites with (●) 0.5 phr BuTPP-MMT and (▲) 1 phr BuTPP-MMT.

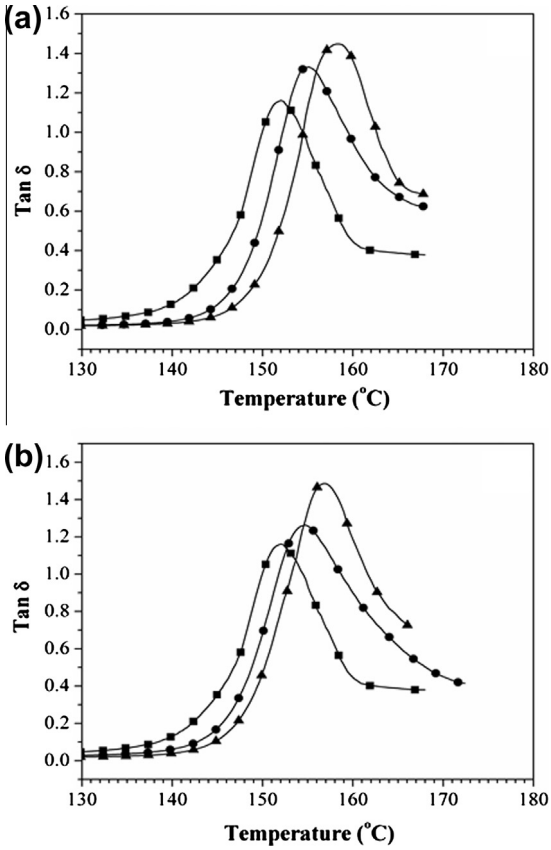

Fig. 14. Tanδ vs. temperature plots of (a) melt blended, (b) solution blended nanocomposites with (●) 0.5 phr BuTPP-MMT, (▲) 1 phr BuTPP-MMT; and (■) represents pure PC in both the cases.

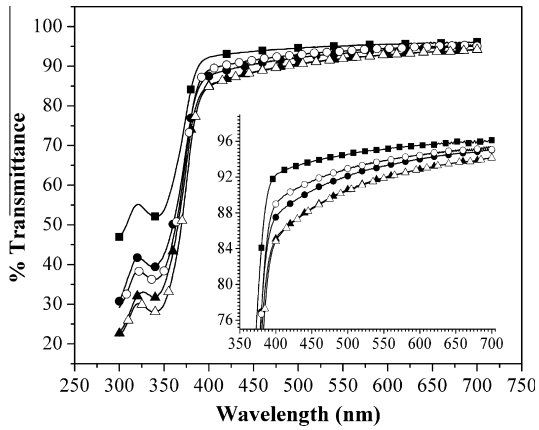

Fig. 15. UV–vis plots of (■) Pure PC, solution-blended PC/BuTPP-MMT nanocomposites with: (●) 0.5 phr clay, (▲) 1 phr clay; melt-blended PC/BuTPP-MMT nanocomposites with: (○) 0.5 phr clay, and (△) 1 phr clay.

the melt and solution blended nanocomposites, at 0.5 phr clay loading. The incorporation of 1 phr clay increased the T_g to ≈157 °C, obeying almost similar trends found previously in DSC analysis.

4.2.7. Optical properties

The optical transparency of the pure PC and the PC/BuTPP-MMT nanocomposites was compared through UV–vis spectroscopic analysis using solid films. Fig. 15 represents the variation in percent transmittance of the melt and solution blended nanocomposites films with similar thickness (thickness 40–50 μm) at varying wavelength (300–700 nm). As observed, the percent transmittance of neat PC (∼96% at 700 nm) was decreased to 95% and 94% respectively on incorporating 0.5 and 1 phr BuTPP-MMT clay into the PC matrix. As the extent of decrease in percent transmittance was almost similar in case of melt and solution blended nanocomposites, the degradation of PC in the melt-blended nanocomposites can be ruled out, and a relatively low optical transparency of the nanocomposites compared to that of the pure PC is due to the refraction in the presence of clay silicate layers into the matrix polymer.

The pure PC and the PC/BuTPP-MMT nanocomposites films were tried to differentiate visually by placing 0.1 mm thick films of the samples on the printed object, as shown in Fig. 16. As observed, both the melt and solution blended nanocomposites films did not give rise to any colour and appeared as visually indistinguishable. The retention of optical clarity in the melt blended PC/BuTPP-MMT nanocomposites could be explained in terms of high stability of the BuTPP-MMT clay against thermal degradation at the processing condition.

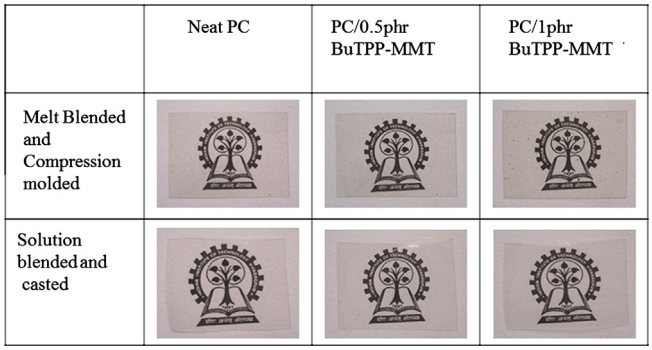

Fig. 16. Photographs of the neat PC and PC/BuTPP-MMT nanocomposites films.

5. Conclusions

Optically transparent PC/BuTPP-MMT nanocomposites with improved mechanical properties have successfully been prepared by industrially feasible melt blending, as well as solution blending techniques. The XRD results revealed a highly exfoliated morphology, irrespective of the amount of clay and blending technique. A more in-depth study of the morphology of the nanocomposites samples through TEM revealed the presence of some zones in which the clay silicate layers were not delaminated very much at higher loading of clay. The thermal stability of the nanocomposites was increased with increase in clay loadings in the PC/BuTPP-MMT nanocomposites. A nominal increase in T_g was found with increase in platelet concentration in the nanocomposites, suggesting free segmental motion of the polymer chains due to the presence an well exfoliated clay morphology. A ∼50% improvement in tensile strength and ∼40% improvement in Young modulus was found at very lower loading (0.5 phr) of the clay. However, the presence of clay in the nanocomposites decreased the extent of elongation at break, originating from the increased brittleness in the nanocomposites. The thermo mechanical investigation revealed an improvement in storage modulus of PC in the PC/BuTPP-MMT nanocomposites. The improved mechanical property, without generation of any colour in the PC/clay nanocomposites may yield up a new era of application of PC in indoor/windows application, headlamp lenses, compact disc, cellular phone, medical applications, etc. with higher performance.

Acknowledgement

S. Suin highly acknowledges Council of Scientific and Industrial Research (CSIR), New Delhi, India for their kind financial support.

References

[1] Ray SS, Okamoto M. Polymer/layered silicate nanocomposites: a review from preparation to processing. Prog Polym Sci 2003;28:1539–641.
[2] Motamedi P, Bagheri R. Investigation of the nanostructure and mechanical properties of polypropylene/polyamide 6/layered silicate ternary nanocomposites. Mater Des 2010;31:1776–84.
[3] Akhlaghi S, Sharif A, Kalaee M, Elahi A, Pirzadeh M, Saeedeh M, et al. Effect of stabilizer on the mechanical, morphological and thermal properties of compatibilized high density polyethylene/ethylene vinyl acetate copolymer/organoclay nanocomposites. Mater Des 2012;33:273–83.
[4] Kashiwagi T, Harris Jr RH, Zhang X, Briber RM, Cipriano BH, et al. Flame retardant mechanism of polyamide 6-clay nanocomposites. Polymer 2004;45:881–91.
[5] Messersmith PB, Giannelis EP. Synthesis and barrier properties of poly(e-capro1actone)- layered silicate nanocomposites. J Polym Sci Polym Chem 1995;33:1047–57.
[6] LeBaron PC, Wang Z, Pinnavaia TJ. Polymer-layered silicate nanocomposites: an overview. Appl Clay Sci 1999;15:11–29.
[7] Sain S, Khatua BB. Synthesis of highly exfoliated PS/Na^+-MMT nanocomposites by suspension polymerization using Na^+-MMT clay platelets as suspension stabilizer. Macromol Res 2011;19:44–52.
[8] Huang X, Lewis S, Brittain WJ, Vaia RA. Synthesis of polycarbonate-layered silicate nanocomposites via cyclic oligomers. Macromolecules 2000;33:2000–4.
[9] Lee KM. Han CD Effect of hydrogen bonding on the rheology of polycarbonate/organoclay nanocomposites. Polymer 2003;44:4573–88.
[10] Yoon PJ, Hunter DL, Paul DR. Polycarbonate nanocomposites. Part 1. Effect of organoclay structure on morphology and properties. Polymer 2003;44:5323–39.
[11] Yoon PJ, Hunter DL, Paul DR. Polycarbonate nanocomposites: Part 2. Degradation and color formation. Polymer 2003;44:5341–54.
[12] Mitsunaga M, Ito Y, Ray SS, Okamoto M, Hironaka K. Intercalated polycarbonate/clay nanocomposites: nanostructure control and foam processing. Macromol Mater Eng 2003;288:543–8.
[13] Hsieh AJ, Moy P, Beyer FL, Madison P, Napadensky E, Ren J, et al. Mechanical response and rheological properties of polycarbonate layered-silicate nanocomposites. Polym Eng Sci 2004;44:825–37.
[14] Nevalainen K, Vuorinen J, Villman V, Suihkonen R, Jarvela P, Sundelin J, et al. Characterization of twin-screw-extruder-compounded polycarbonate nanoclay composites. Polym Eng Sci 2009;9:630–40.

[15] Wu D, Wu L, Zhang M, Wu L. Effect of epoxy resin on rheology of polycarbonate/clay nanocomposites. Eur Polym J 2007;43:1635–44.
[16] Morgan AB, Harris JD. Exfoliated polystyrene-clay nanocomposites synthesized by solvent blending with sonication. Polymer 2004;45:8695–703.
[17] Xie W, Xie R, Pan WP, Hunter D, Koene B, Tan LS, et al. Thermal stability of quaternary phosphonium modified montmorillonites. Chem Mater 2002;14:4837–45.
[18] Wang WS, Liang CK, Chen YC, Su YL, Tsai TY, Chen-Yang YW. Transparent and flame retardant PMMA/clay nanocomposites prepared with dual modified organoclay. Polym Adv Technol 2012;23:625–31.
[19] Calderon JU, Lennox B, Kamal MR. Thermally stable phosphonium-montmorillonite organoclays. Appl Clay Sci 2008;40:90–8.
[20] Avalos F, Ortiz JC, Zitzumbo R, López-Manchado MA, Verdejo R, Arroyo M. Phosphonium salt intercalated montmorillonites. Appl Clay Sci 2009;43:27–32.
[21] Cai Y, Huang F, Xia X, Wei Q, Tong X, Wei A, et al. Comparison between structures and properties of ABS nanocomposites derived from two different kinds of OMT. J Mater Eng Perform 2010;19:171–6.
[22] Rama MS, Swaminathan S. Polycarbonate/clay nanocomposites via in situ melt polycondensation. Ind Eng Chem Res 2010;49:2217–27.
[23] Gilman JW, Awad WH, Davis RD, Shields J, Harris Jr RH, Davis C, et al. Polymer/layered silicate nanocomposites from thermally stable trialkylimidazolium-treated montmorillonite. Chem Mater 2002;14:3776–85.
[24] Xie W, Gao Z, Pan WP, Hunter D, Singh, Vaia R. Thermal degradation chemistry of alkyl quaternary ammonium montmorillonite. Chem Mater 2001;13:2979–90.
[25] Feng J, Hao J, Du J, Yang R. Using TGA/FTIR TGA/MS and cone calorimetry to understand thermal degradation and flame retardancy mechanism of polycarbonate filled with solid bisphenol A bis(diphenyl phosphate) and montmorillonite. Polym Degrad Stab 2012;97:605–14.
[26] Nielsen LE. Models for the permeability of filled polymer systems. J Macromol Sci Chem 1967;1:929–42.
[27] Lape NK, Nuxoll EE, Cussler EL. Polydisperse flakes in barrier films. J Membrane Sci 2004;236:29–37.
[28] Yang C, Smyrl WH, Cussler EL. Flake alignment in composite coatings. J Membrane Sci 2004;231:1–12.
[29] Gusev AA, Lusti HR. Rational design of nanocomposites for barrier applications. Adv Mater 2001;13:1641–3.
[30] Fredrickson GH, Bicerano J. Barrier properties of oriented disk composites. J Chem Phys 1999;110:2181–8.
[31] Choudalakis G, Gotsis AD. Permeability of polymer/clay nanocomposites: a review. Eur Polym J 2009;45:967–84.
[32] Yu YH, Lin CY, Yeh JM, Lin WH. Preparation and properties of poly(vinyl alcohol)-clay nanocomposite materials. Polymer 2003;44:3553–60.
[33] Lu H, Nutt S. Restricted relaxation in polymer nanocomposites near the glass transition. Macromolecules 2003;36:4010–6.
[34] Zheng X, Wilkie CA. Flame retardancy of polystyrene nanocomposites based on an oligomeric organically-modified clay containing phosphate. Polym Degrad Stab 2003;81:539–50.
[35] Suin S, Shrivastava NK, Maiti S, Khatua BB. Phosphonium modified organoclay as potential nanofiller for the development of exfoliated and optically transparent polycarbonate/clay nanocomposites: Preparation and characterizations. Eur Polym J 2013;49:49–60.
[36] Lu C, Mai YW. Influence of aspect ratio on barrier properties of polymer-clay nanocomposites. Phys Rev Lett 2005;95:088303. 1–4.
[37] Mishra JK, Hwang KH, Ha CS. Preparation, mechanical and rheological properties of a thermoplastic polyolefin (TPO)/organoclay nanocomposite with reference to the effect of maleic anhydride modified polypropylene as a compatibilizer. Polymer 2005;46:1995–2002.
[38] Baniasadi H, Ramazani SAA, Javan Nikkhah S. Investigation of in situ prepared polypropylene/clay nanocompositesproperties and comparing to melt blending method. Mater Des 2010;31:76–84.
[39] Venkatesh GS, Deb A, Karmarkar A, Chauhan SS. Effect of nanoclay content and compatibilizer on viscoelastic properties of montmorillonite/polypropylene nanocomposites. Mater Des 2012;37:285–91.
[40] Hasegawa N, Okamoto H, Kawasumi M, Usuki A. Preparation and mechanical properties of polystyrene-clay hybrids. J Appl Polym Sci 1999;74:3359–64.